MOLECULAR IMAGING AND BIOLOGY

Published Online: 10 January 2012

Mol Imaging Biol (2012) 14:608–618
DOI: 10.1007/s11307-011-0537-8

RESEARCH ARTICLE

Positron Emission Tomography of ^{64}Cu-DOTA-Rituximab in a Transgenic Mouse Model Expressing Human CD20 for Clinical Translation to Image NHL

Arutselvan Natarajan,[1] Gayatri Gowrishankar,[1] Carsten H. Nielsen,[1] Sen Wang,[1] Andrei Iagaru,[1] Michael L. Goris,[2] Sanjiv Sam Gambhir[2,3,4]

[1]*Molecular Imaging Program at Stanford, Stanford University, Stanford, CA 94305, USA*
[2]*Division of Nuclear Medicine, Department of Radiology, Stanford University, Stanford, CA 94305, USA*
[3]*Department of Bioengineering, Department of Materials Science and Engineering, Bio-X Program, Stanford University, Stanford, CA 94305, USA*
[4]*Department of Radiology, Stanford University, James H Clark Center E150, 318 Campus Drive, Stanford, CA 94305-5427, USA*

Abstract

Purpose: This study aims to evaluate ^{64}Cu-DOTA-rituximab (PETRIT) in a preclinical transgenic mouse model expressing human CD20 for potential clinical translation.

Procedures: ^{64}Cu was chelated to DOTA-rituximab. Multiple radiolabeling, quality assurance, and imaging experiments were performed. The human CD20 antigen was expressed in B cells of transgenic mice (CD20TM). The mice groups studied were: (a) control (nude mice, n=3) that received 7.4 MBq/dose, (b) with pre-dose (CD20TM, n=6) received 2 mg/kg pre-dose of cold rituximab prior to PETRIT of 7.4 MBq/dose, and (c) without pre-dose (CD20TM, n=6) PETRIT alone received 7.4 MBq/dose. Small animal PET was used to image mice at various time points (0, 1, 2, 4, 24, 48, and 72 h). The OLINDA/EXM software was used to determine the human equivalent dose for individual organs.

Results: PETRIT was obtained with a specific activity of 545±38.91 MBq/nmole, radiochemical purity >95%, and immunoreactivity >75%. At 24 h, spleenic uptake of PETRIT%ID/g (mean± STD) with and without pre-dose was 1.76±0.43% and 16.5±0.45%, respectively (P value= 0.01). Liver uptake with and without pre-dose was 0.41±0.51% and 0.52±0.17% (P value= 0.86), respectively. The human equivalents of highest dose organs with and without pre-dose are osteogenic cells at 30.8±0.4 μSv/MBq and the spleen at 99±4 μSv/MBq, respectively.

Conclusions: PET imaging with PETRIT in huCD20 transgenic mice provided human dosimetry data for eventual applications in non-Hodgkins lymphoma patients.

Key words: ^{64}Cu-rituximab, immunoPET, Radioimmuno imaging

Introduction

Positron emission tomography (PET) has emerged as a clinically important molecular imaging tool in cancer staging and re-staging for a number of malignancies [1]. However, the utility of this approach depends on tracer specificity. Hence, there has been great need and a continued search for imaging agents that are more specific to cancer. This search has driven the development of radiolabeled monoclonal antibodies, proteins, and peptides against tumor-

Correspondence to: Sanjiv Sam Gambhir; *e-mail:* sgambhir@stanford.edu

specific antigens [2, 3]. Targeted radiolabeled imaging agents have been developed mediating antibodies against tumor-specific antigens such as Her2 and carcinoembryonic antigen [4, 5].

The purpose of the current study was to develop and evaluate an antibody-based PET imaging agent for non-Hodgkin's lymphoma (NHL) to monitor lymphoma therapy. NHL is the fifth most common cancer in the US, with 60,000 new cases and approximately 20,000 deaths each year. The incidence of NHL in the United States has increased by 15% over the past two decades, and the cause for this is not known. NHL is a heterogeneous group of diseases of B cell or T cell origin. B cell lymphoma is one of the most prevalent NHL cancers. Although, substantial progress has been made in understanding the molecular pathogenesis of several forms of NHL, prognostic information is based on morphology and histology.

Therefore, we attempted to develop, optimize, and evaluate a novel PET radiopharmaceutical, of an antibody based (rituximab) PET tracer using ^{64}Cu radionuclide (half life, 12.7 h) chelated to 1, 4, 7, 10-tetraazacyclododecane-1, 4, 7, 10-tetraacetic acid (DOTA). Rituximab is murine/human monoclonal IgG1 kappa antibody directed against the CD20 antigen expressing B cell lymphomas and approved by the Food and Drug Administration (FDA) for therapy alone or in combination [6]. DOTA-linked peptides and antibodies are well known to chelate ^{64}Cu with moderate complex stability (K_d 10^{23} M^{-1}) and are also approved by the FDA for clinical studies [7, 8].

The tracer ^{64}Cu-DOTA-rituximab was evaluted using a humanized transgenic B cell lymphoma mouse model in order to monitor lymphoma therapy effectively. This mouse model was used to predict the human dose equivalent from PET imaging for lymphoma therapy monitoring. We based our study on the fact that Rituxan, Bexxar, and Zevalin are all antibodies known to target the CD20 antigen in B cell NHL. The CD20 antigen is a 32-kDa non-glycosylated phosphoprotein, which is commonly expressed by human lymphomas cells, a target in radioimmunotherapy, and over-expressed on the surface of the mature B cells [9, 10].

In the present report, we describe manufacturing, QA, the pre-clinical study, and dosimetry of the novel antibody-based PET radiopharmaceutical against human CD20 prior to translation for NHL patients.

Materials and Methods

Antibody, Cell Lines, and Reagents

The anti-CD20 antibody rituximab was purchased from Stanford University Medical Center pharmacy. Rituximab is a high-affinity chimeric monoclonal antibody of the IgG1 subtype (human κ light chain and human γ1 heavy chain), which recognizes humanized B cell CD20. Ramos, Daudi, and Jurkat cells were obtained from ATCC. Ramos cells were maintained in Dulbecco's modified Eagle's medium (DMEM) (4.5 g/L glucose), Daudi, and Jurkat cells in MEM/Ham's F-12 (1:1) and 1% non-essential amino acids. All media were supplemented with 10% fetal calf serum (FCS), 2 mmol/L glutamine, 100 U/ml penicillin, 100 µg streptomycin, and 0.25 µg/ml fungizone. All media and additives were obtained from Invitrogen Corporation (Carlsbad, CA USA).

Chemicals and solvents used were purchased from Sigma Aldrich (St Louis, MA) unless otherwise stated. High performance liquid chromatography (HPLC) was performed on HPLC-Ultimate 3000 with a SEC 3000 column (Phenomenex, Torrance, CA 90501-1430, USA) with an ultraviolet detector and an online radioactivity detector. *N*-succinimidyl-DOTA (NHS-DOTA) was purchased from Macrocyclics (Dallas, TX, USA). Mass spectrometry (AB SCIEX TOF/TOF 5800) was performed at Stanford University and operated in a linear mode with sinapinic acid matrix.

Preparation of DOTA-Rituximab (Immunoconjugate)

The DOTA-NHS ligand has already shown good biological performance when used in protein conjugation of various radionuclides such as ^{68}Ga, ^{66}Ga, ^{225}Ac, ^{177}Lu, and lead radionuclides [11] DOTA-rituximab immunoconjugate was prepared by using DOTA-NHS [12] linked to rituximab according to published procedures [13, 14]. Briefly, an aqueous solution (125 mmol/L; 10–25 µl) of the ligand (DOTA-NHS) was added to 200 to 400 µl of 0.1 mol/L sodium phosphate buffer (pH 8) containing 3.8 mg (0.025 µmol) of rituximab. The pH was adjusted using saturated solution of Na_3PO_4 to pH 9–10, and the reaction mixture was incubated for 2 h at 25°C. Excess DOTA-NHS was then removed by 30 kDa membrane dialysis using slide-A-lyzer (PIERCE, USA) and buffer exchanged into 0.1 M sodium acetate buffer (pH 5.5) for ^{64}Cu labeling. The immunoconjugates were concentrated by centrifugation-dialysis to 0.1 to 0.2 mg/ml and stored at −80°C. The number of chelators coupled per antibody (c/a) molecule was estimated with MALDI-TOF MS by comparison of rituximab and DOTA-rituximab [15] and by inductively coupled plasma mass spectrometry (ICPMS) using cold copper or isotope dilution assay as described [16, 17].

Radiolabeling of DOTA-Rituximab

The radiolabeling of DOTA-rituximab with $^{64}CuCl_2$ (University of Wisconsin, Madison, WI, USA) was carried out as follows. DOTA-rituximab, 25 to 50 µg in 100 µl of 0.25 mol/L ammonium acetate buffer (pH 5.5) was reacted with 92.5 to 185 MBq of neutralized $^{64}CuCl_2$ solution at 42°C of pH 5.5 for 45 min. After incubation, 0.1 M diethylenetriaminepentaacetic acid (DTPA), pH 7.0 was added to a final concentration of 5 mmol/L and incubated at room temperature for 15 min to scavenge unchelated $^{64}CuCl_2$ in the reaction mixture. Purification of the ^{64}Cu-DOTA-rituximab was achieved by size exclusion liquid chromatography on a Phenomenex SEC 3000 column (Torrance, CA, USA) in PBS buffer [0.1 mol/L NaCl, 0.05 mol/L sodium phosphate (pH 7.4)] with a flow rate of 1.0 ml/min. The radioimmunoconjugate peak (retention time at 7.0 min) corresponding to antibody was collected, concentrated, and filtered through a 0.2-µm filter into a sterile vial.

Immunoreactivity and Stability of the Radiolabeled Immunoconjugates

Each lots of the radioimmunoconjugate preparations were evaluated for their immunoreactivity by cell-binding assays as described by previous publications [18, 19]. Two separate experiments were performed each with and without blocking using cold rituximab (20 and 100 ng/ml). Additions of cold dose were performed 2 h prior to the radiolabeled tracer addition. The same experiments were repeated with all three different cell lines (CD20+: Ramos and Daudi; CD20-: Jurkat) at two different concentrations (20 and 100 ng/ml) of PETRIT tracers. Experiments were performed in triplicates. Briefly, ^{64}Cu-DOTA-rituximab was diluted to 100 and 20 ng/ml concentrations. Dilutions were made in PBS with 2% BSA. To each gamma counter tube, 0.1 ml of cells (1×10^6) and 0.1 ml of PETRIT tracer were added. After addition of tracer, the solutions were gently vortexed and incubated at 37°C. Two hours later, the solutions were centrifuged and the supernatant and pellets were separated. The activities were counted in γ-counter (1470 WIZARD Automatic Gamma Counter; Perkin Elmer, Walthem, MA).

Stability of the labeled antibodies after incubation in human serum at 37°C was analyzed by cellulose acetate electrophoresis (CAE) at 45 min tested at 0, 2, 4, 24, 48, and 72 h [20, 21].

Animal Studies

Animal studies were performed in compliance with approval from the Administrative Panel on Laboratory Animal Care (APLAC) at Stanford University. Nude mice (CD1-nu) from Charles River, Inc, and huCD20 transgenic mice (Genentech, South San Francisco) were used for the experiments. Nude mice and two other groups of human CD20 positive transgenic mice (six animals for each group) were imaged at 0, 0.5, 1, 2, 4, 12, 24, 48, and 72 h using small animal PET at the Stanford small animal imaging center. All experimental mice received ^{64}Cu-labeled radiopharmaceutical [200 µl, corresponding to 7.4 MBq (200 µCi), 2 µg of DOTA-rituximab] via tail vein injection. After radiotracer administration, the animals were scanned at time points indicated above. Results are expressed as percent injected dose per gram of tissue (percent ID per gram). Statistical analysis was done with Student's *t* test (two-tailed, unequal variance).

Small Animal PET Imaging

PET imaging was carried out on a microPET R4 rodent model scanner (Siemens Medical Solutions), as described earlier [22]. Prior to the imaging experiments, the animals (nude and huCD20 transgenic mice) were lightly restrained and administered the dose of ^{64}Cu-DOTA-rituximab (7.4 MBq/2 µg DOTA-rituximab) via a lateral tail vein. At each time points (0, 0.5, 4, 12, 24, 48 and 72 h) the animals were anesthetized with 2% of isoflurane at room temperature and placed in the prone position and near the center of the field of view of the PET scanner. Static scans (1–20 min) were obtained, and the images were reconstructed by use of a two-dimensional ordered subsets expectation maximization (OSEM) algorithm. The calibration constant for ^{64}Cu was determined using a tube containing a known amount of radioactive ^{64}Cu for microPET imaging. The calibration factors for ^{64}Cu are routinely measured and are ~1,732 µCi/ml for our scanner. Animals were at room temperature during the imaging procedure.

Image files were analyzed using the open source software a Medical Image Data Examiner (AMIDE) [23]. For each small animal PET scan, three-dimensional region of interests (ROIs; >5 pixels for coronal and transaxial slices) were drawn over the heart, liver, spleen and whole body on decay-corrected whole-body coronal images. No background correction was performed. The average radioactivity concentration in the region of interest was obtained from mean pixel values within the region of interest volume. These data was converted to counts per ml per minute by using a predetermined conversion factor. The results were then divided by the injected dose to obtain an image region of interest–derived percentage injected dose per cubic centimeter of tissue (% ID/cm^3). No corrections for attenuation or partial volume effect were performed.

Small Animal CT Imaging

CT scans were carried out immediately after microPET, on a small-animal CT scanner without gating (eXplore RS-9 MicroCT, GE Healthcare) at 24, and 48 h. Experiment mice were anesthetized with 2% isoflurane in 2 L/min of oxygen for 6 min in 2 bed positions. Acquisition parameters were as follows: 70-kVp beam energy, 40-mA current, 4.2-cm field of view (z-axis), and 200 projections. EXplore Evolver and eXplore Reconstruction Interface software was used for image acquisition and reconstruction. Images were analyzed using the vendor software (Micro View; GE Healthcare) and AMIDE. The spatial resolution of the images was isotropic at 97 µm.

Dosimetry

The animal organ injected activity data were converted to those for a human using the method of Kirchner *et al.* [24]. The integral of the time activity per organ curve (µCi hr./µCi injected) was determined from the pharmacokinetic data. Dose calculations were done with the OLINDA/EXM version 1 software [25].

Results

Preparation and Characterization of DOTA-Rituximab

The DOTA-rituximab conjugation was achieved by a one-step reaction, and quality assurance was performed using ICPMS, TLC, SEC-HPLC, and MALDI-TOF mass spectrometry. Multiple immunoconjugate lot preparations were made, and each of these lots showed 1–2 DOTA chelates per antibody (c/a), and the final DOTA-rituximab conjugate was greater than 95% monomeric by SEC3000 HPLC, protein peaks measured at UV 280 nm . The MALDI-TOF/TOF mass spectrometry shows the molecular weight of rituximab and DOTA-rituximab are ~148.6 kDa (Fig. 1, trace A) and 149 kDa (Fig. 1, trace B), respectively. The mass difference

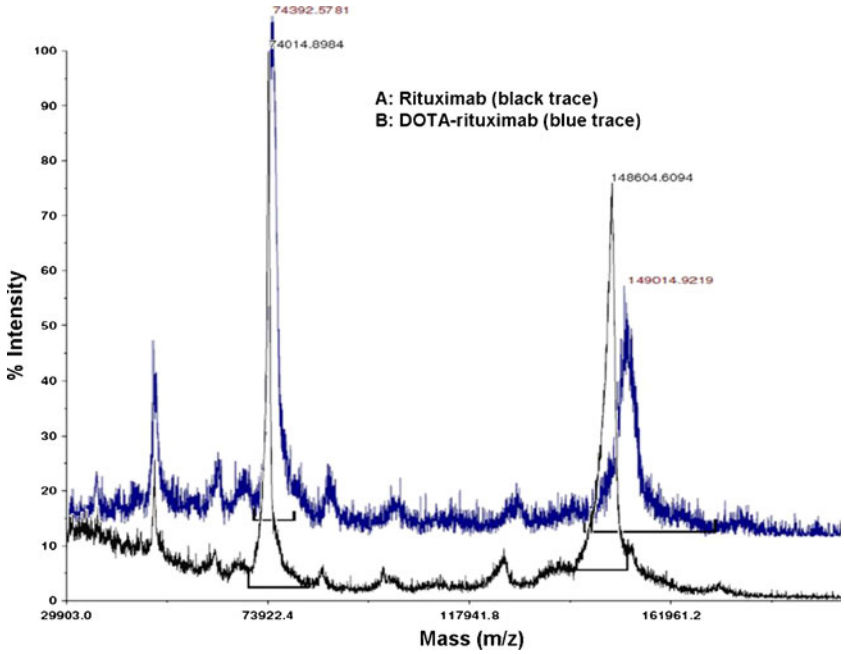

Fig. 1. Estimation of DOTA chelates in rituximab immunoconjugate by mass spectrometry. Comparison of MALDI-TOF MS spectra displaying rituximab unmodified (*black trace*) and DOTA-rituximab modified (*blue trace*). The reaction ratio of rituximab vs. DOTA-NHS was 1:5. Peaks show at *m/z* region of ~150 kDa accounts for 148,604 and 149,014 KDa for rituximab and DOTA–rituximab, respectively. Mass difference between these two peaks of conjugated and DOTA-conjugated rituximab is *m/z* 410 accounts for average one DOTA conjugation per rituximab. Absolute mass of DOTA is 405.2.

between these two peaks at ~150 kDa region accounts for *m/z* 410, this corresponds to one DOTA molecule per rituximab (absolute mass of DOTA *m/z* is 405.2) confirming that the number of DOTA chelates per antibody was at least 1 c/a. This data was further confirmed by ICPMS (data not shown).

Radiolabeling of DOTA-Rituximab

After radiolabeling, the PETRIT yield was in the range of 70–80%. The specific activity was 3.7–4.6 MBq/μg. The radiochemical purity of the final tracer was greater than 95%. The radiotracer radiochemical yield, specific activity, and purity for each of these lot preparations were of consistent quality. Figure 2a shows a typical radio-chromatogram of final dose of radiotracer assayed and used for the animal studies.

In Vitro Cell Binding Study

Table 1 shows the percent binding effect of PETRIT tested with two different concentrations using Ramos and Daudi cells expressing human CD20 and CD20 negative Jurkat cells. The binding effect of the tracer was greater than 75% compared to the binding effect on same cells but pre-blocked with cold rituximab, indicating the tracer retained its immunoreactivity.

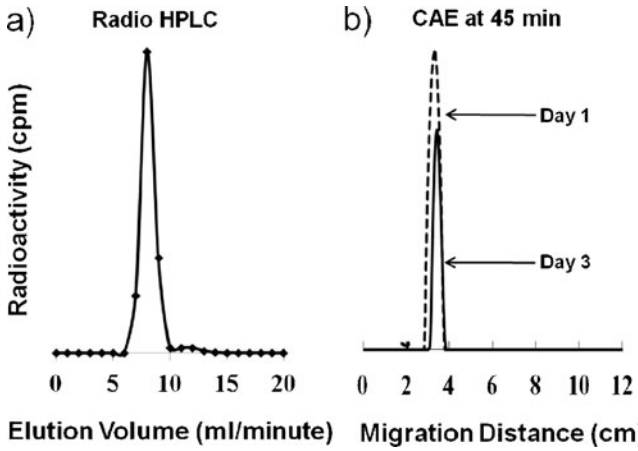

Fig. 2. **a** Radio-HPLC chromatogram of PETRIT shows the purity of the tracer. PETRIT was eluted by SEC 3000 column with a flow rate of 1 ml/min using PBS. Radioactivity of each of 1 ml fractions was measured by gamma counter and the data was used to plot chromatogram by Excel program. **b** Serum stability of PETRIT assayed by cellulose acetate electrophoresis (CAE) at 45 min: The results of serum stability study of ^{64}Cu-DOTA-rituximab tested by CAE are shown. CAE was performed at 45 min with barbital buffer (0.05 M, pH 8.6) at room temperature. Radioconjugate (50 μg) was mixed per ml of human serum and kept at 37°C for 3 days. At various time points (0, 4, 24, 48, and 72 h), 2–10 μl samples were drawn and tested for stability on CAE. Radioactivity peaks in the figure corresponds to radioconjugate in the serum at day 1 and 3 (representative time points), demonstrated radioconjugates are at identical migration distance.

Table 1. Immunoreactivity of ^{64}Cu-DOTA-rituximab was tested with Ramos and Daudi cells (CD20+) and Jurkat cells (CD20−)

Cells (1×10^6)	^{64}Cu-DOTA-rituximab (ng)	Tracer uptake by cells without pre-dose (%)	Tracer uptake by cells with pre-dose (%)
Ramos	10	80.30±0.71	2.31±0.11
	2	79.12±2.36	2.58±0.38
Daudi	10	81.71±0.19	2.31±0.15
	2	79.31±1.80	3.44±0.23
Jurkat	10	7.16±0.57	2.20±0.17
	2	4.64±0.18	3.44±0.23

Experiments were performed in triplicates. The values shown in the table (mean±STD) are tracer uptake by CD20+/− cells tested with and without blocking using cold rituximab

Serum Stability Assay

Figure 2b shows the stability of the radiotracer in human serum over 3 days, tested by CAE at 45 min. The radio peaks in Fig. 2b correspond to radiotracer at each time point. These results showed that the tracer was stable in serum and greater than 98% intact for up to 3 days.

Animal Studies

To evaluate antibody based PET tracer targeting anti-CD20 B-cell lymphoma, we used a humanized transgenic mouse model that expresses CD-20 antigens on B-cells (huCD20 transgenic mouse) developed at Genentech. The huCD20 transgenic mouse model mimics a human B-cell lymphoma tumor and provides a clearance pattern such that rituximab recognize CD-20 antigens on B-cells in human lymphoma patients. Prior to the animal study huCD20 transgenic mice were screened to confirm the expression of CD20 positive targets by RT-PCR. The average weight of the mice was 25.0±2.0 g. The *in vivo* targeting ability of ^{64}Cu-DOTA-rituximab in huCD20 transgenic mice was demonstrated at various time points post tail-vein injection of radiopharmaceutical, with and without blocking of CD20 antigens by cold rituximab. Mice received 7–8 MBq of ^{64}Cu-DOTA-rituximab (mass range, 2–3 μg of rituximab). Each mouse was imaged at various time points (0, 30, 1, 2, 4, 12, 24, 48, and 72 h) after tracer injection.

Small Animal PET and CT Imaging

Figure 3 shows the images that were obtained at 4, 24, and 48 h after injection of tracer. From these images, it is evident that PETRIT had uptake primarily in the spleen. The spleen and liver uptake (percent ID per gram) is given in Fig. 4a, b, at various time points compared with the pre-dose group (human CD20 antigens were pre-blocked with cold rituximab). Figure 4c–d shows the whole body clearance profile of PETRIT for up to 3 days. The radiopharmaceutical uptake (percent ID per gram) in the pre-blocked (n=6) and unblocked (n=6) groups is 1.76±0.43, and 16.5±0.45 for spleen; 0.41±0.51, and 0.52±0.17 for liver, respectively.

Radiation Dose Estimates for Human Patients

The absorbed radiation dose estimates for the administration of PETRIT to humans are shown in Table 2. These results show individual organ doses in humans. The organs with the highest radiation burden (μSv/MBq) with pre-dose administration were osteogenic cells (30.8±0.4), liver (30.4±6.7), and the heart wall (29.4±1.6). Similarly, but without pre-dose administration of cold rituximab, the highest radiation burden (μSv/MBq) dose estimates were for the spleen (99±4), liver (51.2±1. 6), and heart wall (40.1±1.8). The predictable human doses (μSv/MBq) for administration with and without pre-dose with cold rituximab were measured as

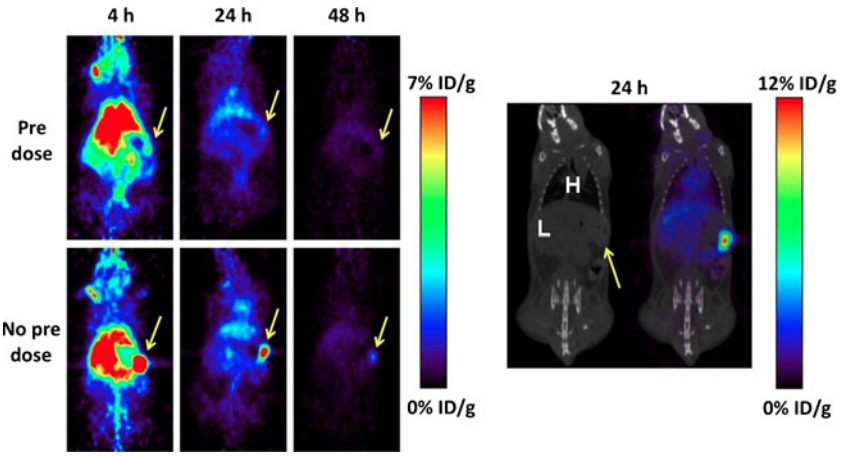

Fig. 3. Small animal PET images of huCD20 mice. The images at *left* are scanned at 4, 24, and 48 h time points after ^{64}Cu-DOTA-rituximab tracer (7.4 MBq) injection; images on *top row* are from a mouse that received 2 mg/kg cold rituximab 2 h prior to tracer injection and bottom row are from a mouse that received the PET tracer only. Images at *right* showed the CT and PET/CT images at 24 h after tracer injection for organ identification. Spleen is indicated by the *yellow arrow*. The other major organs are as marked (*H*=heart and *L*=liver). The *color scale bar* shows tracer%ID/g.

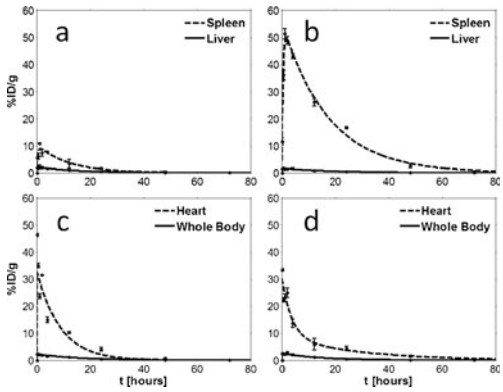

Fig. 4. Clearance profile of ^{64}Cu-DOTA-rituximab tracer (i.v., dose 7.4 MBq) in huCD20 transgenic mice. *Y* axis is percent injected dose per gram (%ID/g) of each organ, and *X* axis is time (*t*) in hours. Figure 4a and c are data from mice that received 2 mg/kg pre-dose of cold rituximab, 2 h prior to tracer injection, and graphs b and d are data from mice that received only the PET tracer. Figure 4a and b are clearance by spleen and liver; Fig. 4c and d are clearance profile of heart and whole body. The data represent the mean±STD of six mice per group.

effective dose (15.8 and 24.7, respectively) and as effective dose equivalent (18.2 and 30.8, respectively).

Table 2. Radiation-absorbed doses were extrapolated to adult male human patient from the ^{64}Cu-DOTA-rituximab injected huCD20 transgenic mouse biodistribution data (with and without pre-dose) using the OLIND/EXM version 1.0 computer program

Radiation dose estimates for adult male (μSv/MBq) using OLINDA		
Organ	Mean absorbed dose±SD	
	With pre-dose	No pre-dose
Adrenals	16.97±0.21	24.10±1.98
Brain	14.00±0.20	19.35±1.77
Breasts	13.73±0.21	19.00±1.70
Gallbladder wall	18.00±0.46	25.60±2.12
LLI wall	16.53±0.25	22.85±2.05
Small intestine	16.90±0.20	23.50±2.12
Stomach wall	16.40±0.17	23.40±1.98
ULI wall	16.80±0.17	23.35±2.05
Heart wall	29.43±1.56	40.05±1.77
Kidneys	16.27±0.15	23.25±1.91
Liver	30.43±6.72	51.20±1.56
Lungs	15.37±0.15	21.50±1.84
Muscle	14.97±0.15	20.75±1.91
Ovaries	16.90±0.20	23.30±2.12
Pancreas	17.43±0.15	25.50±1.98
Red marrow	12.93±0.12	18.00±1.56
Osteogenic cells	30.80±0.40	42.55±3.89
Skin	13.13±0.15	18.15±1.63
Spleen	22.17±0.57	98.50±4.24
Testes	14.80±0.20	20.40±1.84
Thymus	15.63±0.21	21.65±1.91
Thyroid	15.23±0.25	21.05±1.91
Urinary bladder wall	16.40±0.20	22.65±2.05
Uterus	17.00±0.20	23.50±2.12
Total body	15.67±0.21	22.20±1.84
Effective dose equivalent (μSv/MBq)	18.17±0.47	30.80±1.56
Effective dose (μSv/MBq)	15.83±0.32	24.65±1.63

LLI lower large intestine, *ULI* upper large intestine

Discussion

Development of tumor specific imaging agents is very important to accurately stage the patients at initial diagnosis and to evaluate response to specific therapy. Despite several attempts in recent years to find sensitive and specific imaging agents to monitor cancer therapy [26], very few PET agents are in clinical trials [27, 28]. Compared to SPECT, PET is more accurate in terms of quantitative measurement of regional concentration of radiotracers providing superior monitoring of therapy response. Although rituximab-based imaging agents have already been reported using ^{111}In, ^{131}I, and ^{99m}Tc isotopes for SPECT imaging [6, 29], very limited studies have been reported with PET isotopes [30, 31].

To achieve improved sensitivity while maintaining specificity, we have developed a ^{64}Cu-DOTA-rituximab PET tracer (PETRIT) to target CD20 cell surface antigens. In this work, our focus was twofold; first we have optimized the DOTA conjugation and radiochemistry to achieve high specific radioactivity (>4 MBq/μg) and optimal immunoreactivity (>80% immunoreactivity) to detect even the lowest levels of possible huCD20 markers: and second, evaluate the targeting ability of the PETRIT on huCD20 in a transgenic mouse model. Synthesis of PET tracers using ^{64}Cu, with rituximab mAb and rituximab Fab has been attempted elsewhere [30, 31]. Surprisingly, antigen targeting ability of these tracers was not reported *in vitro* or *in vivo* animal imaging. For example, Chan et. al. [31] studied ^{64}Cu-DOTA-rituxmiab Fab as a negative control for HER2 tumor mouse MDA-MB-361 xenograft, and Jalilian et. al. [30] reported only tracer synthesis.

However, in the current study, we presented PETRIT tracer synthesis, quality assurance, serum stability, *in vitro* human lymphoma cell binding assay results, and dosimetry studies using a humanized transgenic mouse model. *In vitro* cell binding assay (Table 1) and *in vivo* mouse imaging (Fig. 3) showed that PETRIT tracer had good binding affinity on CD20 markers both *in vitro* and *in vivo*. Furthermore, the accumulation of tracer on CD20 marker was specific, since blocking with cold rituximab significantly reduces the tracer uptake, both in cell assay, and in *in vivo* imaging studies (Table 1 and Figs. 3 and 4). To the best of our knowledge, this is the first report on dosimetry evaluation of ^{64}Cu-DOTA-rituximab using a huCD20 expressing transgenic mouse model.

In order to evaluate the PETRIT as a novel PET radiopharmaceutical in humans, it was necessary to estimate the radiation dose burden in various organs in animal models prior to human patient studies [32]. Hence, we evaluated the PETRIT dosimetry in small animal PET imaging experiment, and it demonstrated that our PET tracer targeted the CD20 antigen very well. We clearly showed the very high uptake of tracer in spleen of mice which is the antigen sink for CD20 expressing mouse B cells, compared to the group of mice pre-blocked with cold rituximab, confirming the

specific targeting ability of the tracer to the CD20 antigen. The radiotracer specific activity and immunoreactivity of the antibody are high enough, as we were able to see very clear difference in spleen uptake between pre-blocked and unblocked mice. Regarding radioactivity clearance, after 3 days, only the spleen showed ~0.5%ID/g, with undetectable levels in other organs. The pre-blocking with cold rituximab is also practiced clinically during therapy with Zevalin—which is a radiolabeled (^{90}Y labeled) version of a CD20 targeting antibody. The pre-blocking is done clinically to block accumulation of the antibody in one of the antigen sinks which is the spleen. This allows more of the radiolabeled antibody to circulate, thus increasing availability to target lymphoma cells.

The radiation dose of PETRIT absorbed by various organs was evaluated in human CD20 expressing TM mice. After tracer injection, the uptake of tracer in the spleen was high with respect to unblocked (no pre-dose) mice (~15%ID/organ at 24 h after injection). The uptake in the liver was moderate (<4%ID/g) in the beginning and declined gradually thereafter. The high radiotracer uptake in the spleen of unblocked mice is due to the over expression of CD20 antigens by splenic B cells, as the spleen is one of the major source organ for B cells production. Thus, this tracer could be a suitable imaging agent against huCD20-positive lymphomas and can serve as an effective tool for noninvasive *in vivo* monitoring of lymphoma growth and metastasis.

The radiation exposure allowed to research subjects involved in research studies vary within the United States and internationally, as there are three commonly used guidelines available. Firstly, the radioactive drug research committees (RDRCs) operating under the patronage of the US Food and Drug Administration have limits for both effective dose and individual organs, whichever occurs first [33]. Secondly, the National Institutes of Health (NIH) incorporated the effective dose estimates, the proposed radiation risk estimates are considered to be the most accurate measure of radiation risks [33]. Thirdly, the European Commission advocates the guidelines of intermediate risk levels in adults is equivalent to an effective dose range of 1–10 mSv per annum. According to NIH guidelines, the maximum exposure is 50 mSv of effective dose per year for a research subject [34]. Based on the above guidelines, we have estimated the human equivalent dose for PETRIT from the CD20TM small animal study data using Olinda software. For PETRIT, the maximal doses were osteogenic cells (31 μSv, with pre-dose) and spleen (99 μSv without pre-dose). Extrapolating this data for adult male human patients, the maximum activity would be 1.62 and 0.51 GBq, for with and without pre-dose of rituximab, respectively.

Many PET tracers such as ^{18}F-fluorodopa, ^{11}C-hydroxyephedrine, ^{124}I-MIBG, ^{68}Ga-peptides, and ^{86}Y- antibodies have been investigated for tumor imaging. However, except ^{18}F FDG, none of these tracers are in routine use for patient studies. The ^{64}Cu-DOTA-rituximab would be a unique tracer due to the moderate half-life of ^{64}Cu (half-life 12.7 h), and long half-life of the antibody [35] (half-life in human patients, 2–7 days) as well as the specific binding to CD20 expressing B cells. This combination may provide an optimal imaging method to acquire accurate information to estimate and monitor the NHL lesions. This tracer can also likely be directly applied to monitor Zevalin therapy where the current gold standard is imaging with an Indium labeled version of rituximab. Moreover, compared to FDG-PET, ^{64}Cu-DOTA-rituximab PET provides more specific and accurate information due to tracer binding ability at the specific target [36]. In a similar concept, immuno-PET agents were developed [37] with ^{64}Cu-antibody fragments to image CD20 antigen expressing cancers in small animal model demonstrating the potential use of antibody-PET imaging in pre-clinical models; however, using them in humans would require further optimization and FDA approval. Our newly developed PET radiopharmaceutical is ready for clinical translation to CD20 expressing B cell NHL patients and has recently received FDA approval (IND 104995) for imaging such patients to test for safety, dosimetry evaluation, and to monitor therapy. We expect our study outcome of PETRIT tracer may likely be useful to assess the CD20 expression level in NHL human patients prior to radioimmunotherapy. Furthermore, PETRIT tracer might be used to take advantage of the sensitivity of PET in cases of low tumor burden or in cases of indolent lymphomas, in which the sensitivity of ^{18}F-FDG PET can be as low as 50% [33, 38]. Imaging of huCD20 transgenic mouse model could also be used to study responses to therapies in human lymphoma or rheumatoid arthritis, and other autoimmune diseases, *e.g.*, B cell targeting vaccines [39–42].

Conclusions

The pre-clinical evaluation of CD20 targeting ^{64}Cu-DOTA-rituximab in humanized CD20TM showed specific binding to CD20 antigens. The *in vivo* uptake study data clearly demonstrated that the ^{64}Cu-DOTA-rituximab targeted in human B cell expressing spleen in transgenic mice was specific compared to the small animals pre-treated with cold rituximab. The radiation dosimetry estimates obtained from the huCD20TM and extrapolated to humans showed that the radiation doses in most organs in humans would range between 12.9 and 30.8 μSv/MBq with cold rituximab predosing and 18–116 μSv/MBq without pre-dosing. The osteogenic cells (30.8 μSv/MBq) with cold rituximab predosing and spleen (116 μSv/MBq) without pre-dosing were determined to be the dose-limiting organs for adult male human patients. Total predicted dosimetry for human patients are 1.08 and 0.39 GBq annually with and without pre-dose of cold rituximab, respectively. These results suggest that this novel PET radiopharmaceutical ^{64}Cu-DOTA-rituximab has the potential for clinical utility in patients with CD20 expressing B cell NHL. Therefore, clinical studies are planned to evaluate ^{64}Cu-DOTA-rituximab for safety and dosimetry in humans.

Acknowledgements. We thank Drs. Nicholas Van Bruggen at Genentech. We also thank Drs. Fred Chin, David Dick, and the staff in the radiochemistry and cyclotron facilities, the small animal imaging center, and Canary Center at Stanford for Cancer Early Detection for instrumentation support and analysis. This work was supported in part by grants from Genentech (South San Francisco, CA) and NCI ICMIC P50-CA114747 (SSG).

Conflict of interest disclosure. The authors declare no conflict of interests.

References

1. Juweid ME, Cheson BD (2006) Positron-emission tomography and assessment of cancer therapy. N Engl J Med 354:496–507
2. Larson SM (1985) Radiolabeled monoclonal anti-tumor antibodies in diagnosis and therapy. J Nucl Med 26:538–545
3. Wu AM, Yazaki PJ, Tsai S, Nguyen K, Anderson AL, McCarthy DW et al (2000) High-resolution microPET imaging of carcinoembryonic antigen-positive xenografts by using a copper-64-labeled engineered antibody fragment. Proc Natl Acad Sci U S A 97:8495–8500
4. Goldenberg DM, DeLand F, Kim E, Bennett S, Primus FJ, van Nagell JR et al (1978) Use of radio-labeled antibodies to carcinoembryonic antigen for the detection and localization of diverse cancers by external photoscanning. N Engl J Med 298:1384–1388
5. Adams GP, Schier R, McCall AM, Crawford RS, Wolf EJ, Weiner LM et al (1998) Prolonged *in vivo* tumour retention of a human diabody targeting the extracellular domain of human HER2/neu. Br J Cancer 77:1405–1412
6. Cheson BD, Leonard JP (2008) Monoclonal antibody therapy for B-cell non-Hodgkin's lymphoma. N Engl J Med 359:613–626
7. Dearling JL, Voss SD, Dunning P, Snay E, Fahey F, Smith SV, et al (2011) Imaging cancer using PET—the effect of the bifunctional chelator on the biodistribution of a (64)Cu-labeled antibody. Nucl Med Biol 38: 29–38
8. Forrer F, Chen J, Fani M, Powell P, Lohri A, Muller-Brand J et al (2009) *In vitro* characterization of (177)Lu-radiolabelled chimeric anti-CD20 monoclonal antibody and a preliminary dosimetry study. Eur J Nucl Med Mol Imaging 36:1443–1452
9. Zhou X, Hu W, Qin X (2008) The role of complement in the mechanism of action of rituximab for B-cell lymphoma: implications for therapy. Oncologist 13:954–966
10. Glennie MJ, French RR, Cragg MS, Taylor RP (2007) Mechanisms of killing by anti-CD20 monoclonal antibodies. Mol Immunol 44:3823–3837
11. Chappell LL, Dadachova E, Milenic DE, Garmestani K, Wu C, Brechbiel MW (2000) Synthesis, characterization, and evaluation of a novel bifunctional chelating agent for the lead isotopes 203Pb and 212Pb. Nucl Med Biol 27:93–100
12. Chappell LL, Ma D, Milenic DE, Garmestani K, Venditto V, Beitzel MP et al (2003) Synthesis and evaluation of novel bifunctional chelating agents based on 1,4,7,10-tetraazacyclododecane-*N*, *N*′, *N*″, *N*‴-tetraacetic acid for radiolabeling proteins. Nucl Med Biol 30:581–595
13. Li J, Zheng H, Trent J, Bates P, Ng CK (2009) Evaluation of 64Cu-DOTA-AS1411 as a PET tracer for lung cancer imaging. J Nucl Med Meet (Abstracts) 50:1915
14. Li L, Bading J, Yazaki PJ, Ahuja AH, Crow D, Colcher D et al (2007) A versatile bifunctional chelate for radiolabeling humanized anti-CEA antibody with In-111 and Cu-64 at either thiol or amino groups: PET imaging Of CEA-positive tumors with whole antibodies. Bioconjugate Chem 19:89–96
15. Lu SX, Takach EJ, Solomon M, Zhu Q, Law SJ, Hsieh FY (2005) Mass spectral analyses of labile DOTA-NHS and heterogeneity determination of DOTA or DM1 conjugated anti-PSMA antibody for prostate cancer therapy. J Pharm Sci 94:788–797
16. Grunberg J, Novak-Hofer I, Honer M, Zimmermann K, Knogler K, Blauenstein P et al (2005) *In vivo* evaluation of 177Lu- and 67/64Cu-labeled recombinant fragments of antibody chCE7 for radioimmunotherapy and PET imaging of L1-CAM-positive tumors. Clin Cancer Res 11:5112–5120
17. Zimmermann K, Grünberg J, Honer M, Ametamey S, August Schubiger P, Novak-Hofer I (2003) Targeting of renal carcinoma with 67/64Cu-labeled anti-L1-CAM antibody chCE7: selection of copper ligands and PET imaging. Nucl Med Biol 30:417–427
18. Novak-Hofer I, Zimmermann K, Maecke HR, Amstutz HP, Carrel F, Schubiger PA (1997) Tumor uptake and metabolism of copper-67-labeled monoclonal antibody chCE7 in nude mice bearing neuroblastoma xenografts. J Nucl Med 38:536–544
19. Lindmo T, Boven E, Cuttitta F, Fedorko J, Bunn PA Jr (1984) Determination of the immunoreactive fraction of radiolabeled monoclonal antibodies by linear extrapolation to binding at infinite antigen excess. J Immunol Methods 72:77–89
20. Saludes JP, Natarajan A, DeNardo SJ, Gervay-Hague J (2010) The remarkable stability of chimeric, sialic acid-derived alpha/delta-peptides in human blood plasma. Chem Biol Drug Des 75:455–460
21. Adams GP, DeNardo SJ, Deshpande SV, DeNardo GL, Meares CF, McCall MJ et al (1989) Effect of mass of 111In-benzyl-EDTA monoclonal antibody on hepatic uptake and processing in mice. Cancer Res 49:1707–1711
22. Schipper ML, Cheng Z, Lee SW, Bentolila LA, Iyer G, Rao J et al (2007) microPET-based biodistribution of quantum dots in living mice. J Nucl Med 48:1511–1518
23. Loening AM, Gambhir SS (2003) AMIDE: a free software tool for multimodality medical image analysis. Mol Imaging 2:131–137
24. Kirschner AS, Ice RD, Beierwaltes WH (1973) Radiation dosimetry of 131I-19-iodocholesterol. J Nucl Med 14:713–717
25. Stabin MG, Siegel JA (2003) Physical models and dose factors for use in internal dose assessment. Heal Phys 85:294–310
26. Dunphy MP, Lewis JS (2009) Radiopharmaceuticals in preclinical and clinical development for monitoring of therapy with PET. J Nucl Med 50(Suppl 1):106S–121S
27. Dijkers EC, Kosterink JG, Rademaker AP, Perk LR, van Dongen GA, Bart J et al (2009) Development and characterization of clinical-grade 89Zr-trastuzumab for HER2/neu immunoPET imaging. J Nucl Med 50:974–981
28. Dijkers EC, Oude Munnink TH, Kosterink JG, Brouwers AH, Jager PL, de Jong JR et al (2010) Biodistribution of 89Zr-trastuzumab and PET imaging of HER2-positive lesions in patients with metastatic breast cancer. Clin Pharmacol Ther 87:586–592
29. Conti PS, White C, Pieslor P, Molina A, Aussie J, Foster P (2005) The role of imaging with 111In-ibritumomab tiuxetan in the ibritumomab tiuxetan (zevalin) regimen: results from a zevalin imaging registry. J Nucl Med 46:1812–1818
30. Jalilian AR, Mirsadeghi L, Yari-Kamrani Y, Rowshanfarzad P, Kamali-Dehghan M, Sabet M (2007) Development of [Cu-64]-DOTA-anti-CD20 for targeted therapy. J Radioanal Nucl Chem 274:563–568
31. Chan C, Scollard D, McLarty K, Smith S, Reilly R (2011) A comparison of 111In- or 64Cu-DOTA-trastuzumab Fab fragments for imaging subcutaneous HER2-positive tumor xenografts in athymic mice using microSPECT/CT or microPET/CT. EJNMMI Res 1:15
32. Dixit R, Boelsterli UA (2007) Healthy animals and animal models of human disease(s) in safety assessment of human pharmaceuticals, including therapeutic antibodies. Drug Discov Today 12:336–342
33. Tsukamoto N, Kojima M, Hasegawa M, Oriuchi N, Matsushima T, Yokohama A et al (2007) The usefulness of (18)F-fluorodeoxyglucose positron emission tomography ((18)F-FDG-PET) and a comparison of (18)F-FDG-pet with (67)gallium scintigraphy in the evaluation of lymphoma: relation to histologic subtypes based on the World Health Organization classification. Cancer 110:652–659
34. (1996) Radiological protection and safety in medicine. Annals of the ICRP 26: 1–31
35. McLaughlin P, Grillo-Lopez AJ, Link BK, Levy R, Czuczman MS, Williams ME et al (1998) Rituximab chimeric anti-CD20 monoclonal antibody therapy for relapsed indolent lymphoma: half of patients respond to a four-dose treatment program. J Clin Oncol 16:2825–2833
36. Smith-Jones PM, Solit D, Afroze F, Rosen N, Larson SM (2006) Early tumor response to Hsp90 therapy using HER2 PET: comparison with 18F-FDG PET. J Nucl Med 47:793–796
37. Olafsen T, Sirk SJ, Betting DJ, Kenanova VE, Bauer KB, Ladno W et al (2010) ImmunoPET imaging of B-cell lymphoma using 124I-anti-CD20 scFv dimers (diabodies). Protein Eng Des Sel 23:243–249
38. Karam M, Novak L, Cyriac J, Ali A, Nazeer T, Nugent F (2006) Role of fluorine-18 fluoro-deoxyglucose positron emission tomography scan in the evaluation and follow-up of patients with low-grade lymphomas. Cancer 107:175–183

39. Betting DJ, Kafi K, Abdollahi-Fard A, Hurvitz SA, Timmerman JM (2008) Sulfhydryl-based tumor antigen-carrier protein conjugates stimulate superior antitumor immunity against B cell lymphomas. J Immunol 181:4131–4140
40. Gong Q, Ou Q, Ye S, Lee WP, Cornelius J, Diehl L et al (2005) Importance of cellular microenvironment and circulatory dynamics in B cell immunotherapy. J Immunol 174:817–826
41. Ahuja A, Shupe J, Dunn R, Kashgarian M, Kehry MR, Shlomchik MJ (2007) Depletion of B cells in murine lupus: efficacy and resistance. J Immunol 179:3351–3361
42. Mease PJ (2008) B cell-targeted therapy in autoimmune disease: rationale, mechanisms, and clinical application. J Rheumatol 35:1245–1255